Measurement of contact-line dissipation in a nanometer-thin soap film

Shuo Guo, Chun Huen Lee, Ping Sheng, and Penger Tong*
Department of Physics, Hong Kong University of Science and Technology, Clear Water Bay, Kowloon, Hong Kong
(Received 17 September 2014; published 14 January 2015)

We report a direct measurement of the friction coefficient ξ_c of two fluctuating contact lines formed on a fiber surface when a long glass fiber intersects the two water-air interfaces of a thin soap film. The glass fiber of diameter d in the range of 0.4–4 μm and length 100–300 μm is glued onto the front end of a rectangular cantilever used for atomic force microscopy. As a sensitive mechanical resonator, the hanging fiber probe can accurately measure a minute change of its viscous damping caused by the soap film. By measuring the broadening of the resonant peak of the hanging fiber probe with varying viscosity η of the soap film and different surface treatments of the glass fiber, we confirm that the contact line dissipation obeys a universal scaling law, $\xi_c = \alpha\pi d\eta$, where the coefficient $\alpha = 1.1 \pm 0.3$ is insensitive to the change of liquid-solid contact angle. The experimental result is in good agreement with the numerical result based on the phase field model under the generalized Navier boundary conditions.

DOI: 10.1103/PhysRevE.91.012404 PACS number(s): 68.08.−p, 83.50.Lh, 83.85.Vb, 05.40.−a

I. INTRODUCTION

The dynamics of a moving contact line (MCL) between a liquid interface and a solid surface is an outstanding problem in fluid physics and has been with us for many years [1–4]. The motion of the contact line is a singular problem, as it is incompatible with the nonslip boundary condition and would lead to unphysical infinite dissipation [5]. Over the years there have been many models and proposals aimed at resolving the incompatibility issue [1–4]. As illustrated in the inset of Fig. 1(a), the MCL involves fluid motion (i) at a small distance a ($\sim$1 nm) in the immediate vicinity of the contact line, in which molecular interactions between the liquid and solid are important, and (ii) in the "outer region" of meso- or macroscopic size L, in which classical hydrodynamics are applicable. Most experiments on MCL were conducted in regime (ii) [6–8], because direct observation of the fluid motion in regime (i) ($\lesssim$1 μm) is difficult with the conventional optical methods. While these measurements provided useful information about the MCL dynamics at large distances, direct comparison of the experimental results with the microscopic models of MCL in regime (i) is difficult.

As a result, our current understanding of the contact line dynamics in regime (i) relies mainly on the results from molecular dynamic simulations [9–12]. These simulations, however, were carried out under highly idealized conditions, such as atomically smooth solid surface and simplified fluid-solid interactions. Direct measurement of the properties of the MCL in regime (i) is, therefore, needed in order to test different theoretical ideas. Understanding the contact line motion is also relevant to many industrial processes ranging from spreading of droplets, lubricants, and coatings to the extraction of oil from sandstone by injecting water or gas [3].

In a recent experiment [13], we used a newly developed hanging fiber probe [14] based on atomic force microscopy (AFM) to directly measure the friction coefficient ξ_c of a fluctuating contact line. As shown in Fig. 1(b), the "long needle" AFM involves a vertical glass fiber of diameter d in the range of 0.4–4 μm and length 100–300 μm, which is glued onto the front end of a rectangular AFM cantilever. As a sensitive mechanical resonator, the hanging fiber probe can accurately measure a minute change of its viscous damping, when the fiber tip just barely touches a liquid-air interface, at which a circular contact line between the interface and the fiber surface is formed. The friction coefficient ξ_c is obtained through the measurement of the resonant power spectrum of fluctuation amplitude of the contact line at equilibrium (no external driving), which is amplified under the spontaneous resonance condition. The contact line fluctuations referred to here are thermal fluctuations of the contact line about its equilibrium position on the fiber surface. Even when the contact line is macroscopically pinned by physical roughness or chemical heterogeneity on the surface, it can still fluctuate microscopically around the energy minimum of the complex defect landscape experienced by the contact line. The fluctuation and dissipation are intrinsically linked together by the fluctuation-dissipation theorem [15], which establishes what happens at the microscopic level to a macroscopically measurable dissipation coefficient.

Previously, by measuring the broadening of the resonant peak of the hanging fiber cantilever system with varying liquid viscosity η, we found that ξ_c obeys a scaling law [13],

$$\xi_c = \alpha\pi d\eta, \tag{1}$$

where πd is the contact line length and $\alpha = 0.8 \pm 0.2$ is a numerical constant independent of the liquid-solid contact angle. This universal scaling law applicable to liquids with different viscosities, surface tensions, and contact angles was further supported by the numerical simulation [13] based on the phase field model under the generalized Navier boundary conditions [11,16,17]. The obtained numerical value of α is in good agreement with the experimental value.

Like many interfacial phenomena, the measurement of viscous damping involves contributions from the bulk fluid. In our previous case, the measured total friction coefficient ξ has three terms:

$$\xi = \xi_e + \xi_s + \xi_c, \tag{2}$$

*penger@ust.hk

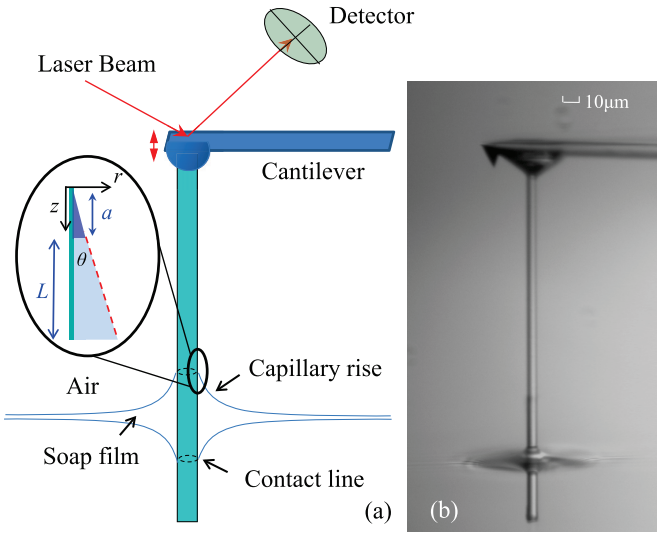

FIG. 1. (Color online) (a) Sketch of the AFM-based hanging fiber resonator intersecting a thin soap film. The dashed circles show the two contact lines formed on each side of the soap film. Inset shows the geometry near the contact line and the coordinate system used in the experiment. (b) A microscope picture of a glass fiber of diameter $d = 4\,\mu$m and length 300 μm intersecting a thin soap film.

where ξ_e is the contribution from the end surface of the fiber, ξ_s is the contribution from the sidewall, and ξ_c is the contribution from the fluctuating contact line. By using a micron-sized glass fiber and keeping the fiber tip at the minimum contact with the liquid interface, we were able to measure ξ_c after the contributions from ξ_e and ξ_s were subtracted.

In this paper, we report a new experiment to directly measure the contact line friction ξ_c without any corrections from the end surface or sidewall. This is achieved by using a thin free-standing soap film. When the hanging fiber intersects the soap film, two contact lines form on the fiber surface with the two water-air interfaces of the soap film and no end surface is made, as illustrated in Fig. 1(a). The measured ξ_c is found to decrease with time as the aqueous solution in the soap film gradually drains out and reaches an asymptotic value when the film thickness becomes very small ($\lesssim$35 nm). As the asymptotic film thickness ($\lesssim$35 nm) sets an upper limit to the viscous contributions from regime (ii), the present experiment is able to focus on the microscopic drag of the contact line in regime (i) (to be further elaborated below). The obtained asymptotic value of ξ_c is found to be twice as large as that predicted by Eq. (1), owing to the existence of two contact lines in the present case.

The remainder of the paper is organized as follows. We first describe the basic working principle of the hanging fiber probe in Sec. II. The experimental procedures and sample preparation methods are presented in Sec. III. The experimental results and discussions are given in Secs. IV and V. Finally, the work is summarized in Sec. VI.

II. THEORETICAL BACKGROUND

The vertical displacement $z(t)$ of the glass fiber ($\equiv$ vertical deflection of the AFM cantilever) is well described by the Langevin equation [14,18]:

$$m\frac{\partial^2 z}{\partial t^2} + \xi\frac{\partial z}{\partial t} + kz = f_B(t), \tag{3}$$

where m is the effective mass of the modified cantilever, $\xi\partial z/\partial t$ is the drag force on the fiber with ξ being the friction coefficient, $kz(t)$ is the elastic force due to the bending of the cantilever with a spring constant k, and $f_B(t)$ is the random Brownian force due to thermal fluctuations of the surrounding fluid. While $f_B(t)$ has a zero mean, its root-mean-square value, $\langle f_B^2\rangle = 2k_BT\xi$, is a nonzero quantity with k_BT being the thermal energy of the system [19].

The measurable quantity in the experiment is the power spectrum, $|z(\omega)|^2$ (or equivalently $|z(f)|^2$), of vertical deflections $z(t)$, which can be solved analytically from Eq. (3) [14,18]:

$$|z(\omega)|^2 = \frac{2k_BT\xi/m^2}{\left(\omega^2-\omega_0^2\right)^2 + (\omega\xi/m)^2}, \tag{4}$$

where $\omega = 2\pi f$ is the angular frequency and $\omega_0 = (k/m)^{1/2}$ ($\sim$600 kHz) is the resonant frequency of the system. Being operated at a resonant state, the hanging fiber amplifies the fluctuation spectrum and thus can accurately detect a minute change in ξ caused by the extra damping from a thin soap film. Because of the high resonant frequency, the technique itself also acts as a narrow bandpass filter, which removes much of the unwanted noise of electronic origin and from low-frequency surface (capillary) waves (see more discussions in Sec. V below).

The hanging fiber resonator has been thoroughly tested in two recent experiments [14,20]. It was found that the measured resonant power spectrum $|z(\omega)|^2$ is well described by Eq. (4), and the resulting friction coefficient $\xi(h)$ as a function of the immersion length h of the fiber in the liquid phase agrees with the theoretical predictions [14]. In addition, the hanging fiber probe was used to measure the fluid viscosity η and the obtained values of η for aqueous solutions of glycerin with varying mass concentrations from 0 wt.% (pure water) to 50 wt.% agree well with those obtained directly by a commercial rheometer [20]. These results thus demonstrated that the use of the hanging fiber probe together with the fluctuation-dissipation theorem to measure the friction coefficient ξ at equilibrium works.

III. EXPERIMENT

A. Preparation of soap films

The soap solution is prepared by mixing a commercial detergent (Ultra Joy Dishwashing Liquid) with a solution of glycerine and deionized water. For all the solutions used in the experiment, the amount of the dishwashing detergent added is 1 wt.%. The viscosity η of the soap solution thus depends only on the amount of glycerine in the aqueous solution and is not affected much by the detergent. By varying the mass concentration of glycerine from 20 to 65 wt.%, the value of η changes from 1.65 to 13.7 cP.

A glass pipette containing the soap solution is used to blow bubbles, which are then transferred to a supporting frame for the AFM measurement. Two types of supporting frames are

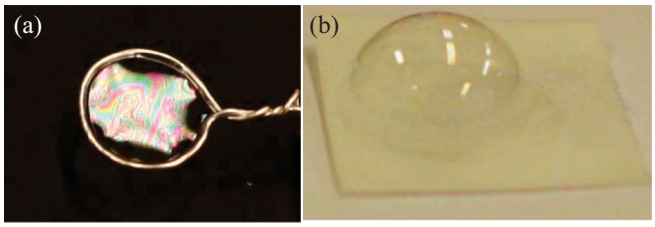

FIG. 2. (Color online) Two soap film holders used in the experiment. (a) A metal ring of diameter 1 cm is used to support the soap film. (b) A soap bubble formed on a 1 cm × 1 cm filter paper.

used to hold the soap film and control its drainage. First, a metal ring of diameter 1 cm is used to support the soap film, as shown in Fig. 2(a). The draining of the soap film takes place along the metal ring to a plastic container on the bottom (not shown). It is found that the steady-state thickness ℓ of the soap film varies from $\sim$5 μm to $\sim$10 nm. Soap films with a higher viscosity tend to be thicker. To obtain a high viscosity thin film with ℓ in the range of 30–10 nm, one needs to increase the draining speed of the soap film. This is achieved by using a filter paper as a supporting substrate, on which a soap bubble is formed as shown in Fig. 2(b). The filter paper is soaked with the same soap solution and the amount of soap solution in the filter paper controls the draining speed. A filter paper that is dry or soaked with a little amount of soap solution drains the film faster. On the contrary, a filter paper soaked with a large amount of soap solution slows down the draining. While the soap film on the two supporting frames has a different shape, we find no difference in the measurements of both the capillary force and friction coefficient using the two types of soap films. This is because the radius of curvature of the soap film formed on the filter paper is much larger than the micron-sized hanging fiber probe. As a result, the large radius of curvature of the soap bubble does not affect our measurements.

The thickness of the soap film is measured using a UV-visible spectrophotometer (Lambda 20, PerkinElmer), following the standard procedure [21]. The spectrophotometer uses the interference effect between the transmitted and reflected lights to measure the film thickness. This is achieved by measuring the absorption spectrum of a beam of light passing through a transparent film as a function of the wavelength of the light beam. The thickness ℓ of the film is obtained when the index of refraction of the film is known. The minimum thickness of the soap film measurable with this apparatus is 35 nm.

B. Surface treatment of glass fibers

Three glass fibers with different surface treatments are used in the experiment. The first is the plasma-cleaned bare glass fiber with a contact angle $\theta \simeq 0^\circ$. The second glass fiber is coated with a monolayer of dipalmitoylphosphatidylcholine (DPPC) using the Langmuir-Blodgett method. DPPC is a phospholipid consisting of two palmitic acid chains [22]. To test the stability of the DPPC monolayer, we measure the capillary force versus displacement curve in water using the same DPPC-coated fiber both before and after the experiment with a soap film. The measured force curves are found to be identical, indicating that the DPPC monolayer remains unchanged during the experiment with the soap film. The third glass fiber is coated with a monolayer of trichloro(1H,1H,2H,2H-perfluorooctyl)silane (FTS), which is covalently grafted on the fiber surface [23,24]. The latter two surfaces are hydrophobic and have an (advancing) contact angle of 83° and 95°, respectively, with the water-air interface. For the soap films, however, because of the adsorption of the surfactant molecules on the fiber surface and the high surfactant concentration of the liquid interface, the DPPC- and FTS-coated fiber surfaces become more hydrophilic; the DPPC-coated fiber has a contact angle $\theta \simeq 0^\circ$ and the FTS-coated fiber has a contact angle $\theta \simeq 20^\circ$.

C. AFM operation

Figure 1(b) shows a microscope picture of a hanging glass fiber of diameter $d = 4\,\mu$m and length 300 μm intersecting a thin soap film. Two capillary rises form around the fiber surface and they are symmetrically aligned on the two sides of the soap film. The two capillary rises change the reflection of light, as observed under a microscope. The assembly of the hanging fiber probe is carried out under a high-magnification stereo-microscope using a motorized micromanipulator system. The thin glass fiber is pulled out of a capillary glass rod of diameter 1.0 mm using a pippette puller. An UV-curable glue (Norland, NOA 81) is used to permanently connect the glass fiber to the front end of a rectangular tipless cantilever beam. Typically, glass fibers of diameter d in the range of 0.4–4 μm and length 100–300 μm are used in the experiment. More details about the assembly of the hanging fiber and its surface treatment have been described elsewhere [14].

The AFM sample cell holding the soap film is mounted on a motor-controlled stage, which moves vertically with an accuracy of 0.1 μm. When the glass fiber tip touches the soap film, a capillary force is detected by the AFM sensor. This makes the determination of the contact point between the fiber tip and the soap film to be accurate to within 0.1 μm. Measurements of $|z(f)|^2$ are conducted using an AFM (MFP-3D, Asylum Research Inc.) operated under the thermal power spectral density (PSD) mode. Typically, $|z(f)|^2$ is taken with a frequency resolution of 152 Hz and the averaging time for each $|z(f)|^2$ is set for $\sim$1 min. To determine the absolute value of $|z(f)|^2$, the output voltage signal from the position-sensitive detector is calibrated against known values of the cantilever deflection. It is found that the experimental uncertainties of the measured $|z(f)|^2$ can be kept at the level of 5–10%.

IV. EXPERIMENTAL RESULTS

A. Measurement of capillary force

The hanging fiber shown in Fig. 1 is also an accurate force sensor capable of measuring the capillary force,

$$f = \pi d\gamma \cos\theta, \tag{5}$$

acting on the contact line of length πd, which is formed on the fiber surface with a *single* liquid interface of surface tension γ and contact angle θ. With an accurate calibration of the cantilever, the AFM can measure the capillary force down to $\sim$10 pN at the accuracy of 0.2%. Figure 3(a) shows

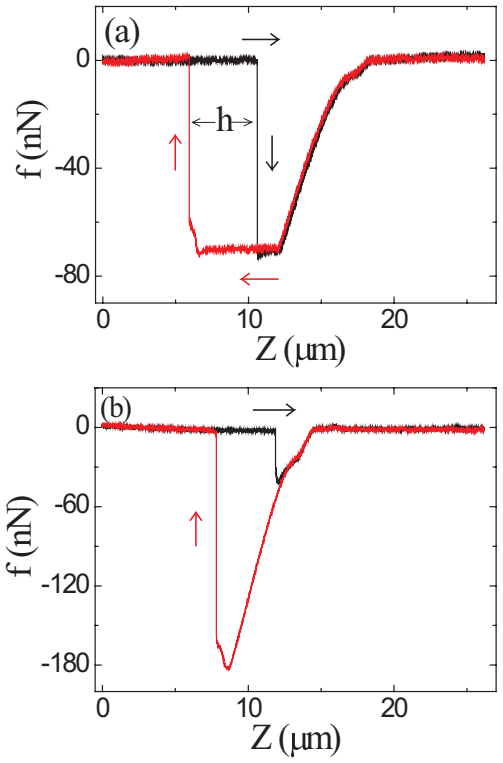

FIG. 3. (Color online) (a) Recorded time evolution of the measured capillary force f when a glass fiber pierces through a thicker soap film with $\ell \simeq 1.6\,\mu$m. (b) Same process for a thinner soap film with $\ell < 35$ nm. The black curves ($\rightarrow$) are measured when the glass fiber is pushed downward at a constant speed $U = 10\,\mu$m/s. The red curves ($\leftarrow$) are obtained when the glass fiber is pulled back upward at the same speed.

a typical time evolution curve of the measured f, when a glass fiber pierces through a soap film. The black curve ($\rightarrow$) shows how the measured f changes when the glass fiber is pushed downward at a constant speed $U = 10\,\mu$m/s. Once the fiber tip touches the upper surface of the soap film at $Z \simeq 10.6\,\mu$m, a capillary force of $f \simeq 70$ nN is detected. The minus sign indicates that the capillary force pulls down the fiber ($\theta < 90^\circ$). In a separate experiment, we measure the values of θ and γ using the hanging fiber probe in contact with a drop of soap solutions, of which the soap film is made. From the measured capillary force, we find the contact angle $\theta = 0^\circ$ and surface tension $\gamma = 23.2$ mN/m for all the soap solutions on a cleaned glass fiber. For a thick soap film (with film thickness $\ell \simeq 1.6\,\mu$m) as shown in Fig. 3(a), we find that when the fiber tip just touches the upper surface of the soap film, the measured value of f agrees well with that obtained from the soap solution, confirming our expectation that the values of θ and γ for the soap film should be the same as those for the soap solution, as it is made from the same solution.

As the fiber continues to move downward and touches the lower surface of the soap film at $Z \simeq 12.2\,\mu$m, another contact line forms on the fiber with an initial contact angle $\theta_l = 90^\circ$. Now the total force acting on the fiber is, $f = \pi d\gamma(1 - \cos\theta_l)$, resulting from the two capillary forces of opposite signs. As the fiber further moves downward, the value of θ_l decreases and reaches its equilibrium value, $\theta_l \simeq 0^\circ$, at $Z \simeq 18.2\,\mu$m. Thus, the total force is canceled out and we have $f = 0$. This is shown in Fig. 3(a) for $Z \geqslant 18.2\,\mu$m. In this case, the fiber is under zero external force, as if it is in air.

The red curve ($\leftarrow$) in Fig. 3(a) shows the time evolution of the measured f when the glass fiber is pulled back upward at the same speed U. The value of f starts to decrease from zero when the fiber tip retracts back to the lower surface of the soap film at $Z \simeq 18.2\,\mu$m. As the fiber further moves upward, the contact angle θ_l of the lower capillary rise changes continuously from 0° to 90° and finally the lower surface snaps off from the fiber tip. The maximum force measured is $f = \pi d\gamma$ when only the upper surface of the soap film is in contact with the fiber at the contact angle $\theta \simeq 0^\circ$. It is found that the measured f remains unchanged when the moving speed U of the fiber is changed from 0.1 to 100 μm/s. The distance h ($\simeq$4.7 μm) between the black and red vertical lines in Fig. 3(a) gives the height of the capillary rise on the upper side of the soap film.

It is seen from Fig. 3(a) that there is a small but reproducible step in the measured force curves when the fiber tip intersects with either the top or bottom interfaces of the soap film. This small step is caused by surface defects at the fiber tip. During the assembly of the hanging fiber probe, a centimeter-long glass fiber was first glued onto the AFM cantilever. The fiber was then cut at a desired length using a homemade scissors-like cutter, whose sharpest edge is about 20 μm in width. In this case, the fiber was actually broken apart, so that the fiber tip sometimes has defects, such as a nonflat surface.

For a thick film as shown in Fig. 3(a), there is a plateau region in the black curve and the width of the plateau region is the soap film thickness $\ell \simeq (12.2 - 10.6)\,\mu\text{m} = 1.6\,\mu$m. If the film thickness is much smaller than 1 μm, as shown in Fig. 3(b), there is no well-developed plateau region and one only observes a short transient of the capillary force development when the fiber tip pierces through the soap film. In this case, one can still obtain the height h of the capillary rise but not the thickness ℓ of the soap film.

For thinner films, we use the UV-visible spectrophotometer to measure the soap film thickness ℓ. Figure 4 shows the time evolution of ℓ as the aqueous solution in the soap film gradually drains out. The viscosity of the soap film is $\eta = 1.65$ cP and

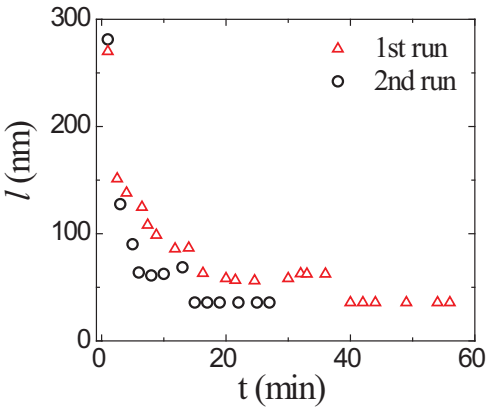

FIG. 4. (Color online) Measured soap film thickness ℓ as a function of draining time t. The measurements are repeated twice (black circles and red triangles) using a UV-visible spectrophotometer.

the measurements of ℓ are repeated twice (black open circles and red triangles). It is seen that the value of the measured ℓ decreases with time and reaches the resolution limit of the spectrophotometer, which is 35 nm, after 20 min. While the apparent value of ℓ saturates at 35 nm after 20 min, the actual film thickness continues to decrease for another ~40 min when the soap film becomes black with ℓ in the range of 35–5 nm [25,26] until it finally bursts. Note that in the spectrum measurements, the soap film is orientated vertically for a horizontally aligned light beam to go through. In the AFM measurements to be described below, the soap film is held horizontally. Therefore, the time-dependence of the measured ℓ as shown in Fig. 4 can only serve as a rough guide.

B. Measurement of contact line dissipation

In the measurement of the power spectrum $|z(f)|^2$, the hanging fiber is kept still after it pierces through the soap film with a penetrating tip of ~10 μm in length, which is long enough for the two capillary rises to form. The measured $|z(f)|^2$ remains unchanged if the fiber is pushed through the soap film with different penetrating length. Each $|z(f)|^2$ is obtained right after the fiber pierces through the soap film and the time taken for collecting data is less than 1 min. The fiber is then pulled out of the soap film and waits for the next measurement at a later time. Figure 5(a) shows an example of the measured $|z(f)|^2$ when a glass fiber intersecting a thin soap film with $\eta = 1.65$ cP (black circles). The measured $|z(f)|^2$ is well described by Eq. (4), as shown by the solid line in Fig. 5(a). It is found that the draining of the soap film also affects the friction coefficient ξ. From the measured $|z(f)|^2$ at different draining times t, we obtain the fitted value of $\xi(t)$ as a function of draining time t. We also measure $|z(f)|^2$ when the fiber is in air and obtain the corresponding friction coefficient ξ_a, which is independent of time.

Figure 5(b) shows the time evolution of the net friction coefficient $\Delta\xi(t) \equiv \xi(t) - \xi_a$, normalized by $\pi d\eta$. Similar to the time evolution of the film thickness ℓ, the measured $\Delta\xi(t)$ decreases with the draining time t and reaches an asymptotic value after 20 min when the film thickness becomes thin enough ($\ell < 35$ nm), so that the measured $\Delta\xi$ is independent of ℓ. The measured asymptotic value $\Delta\xi_\infty$ agrees well with the prediction of Eq. (1), which states that $\Delta\xi_\infty/(\pi d\eta) = 2\alpha$ with $\alpha = 1.1$ (dashed line), where the factor of 2 accounts for the two contact lines in the soap film. From Fig. 5(b) we conclude that the friction coefficient ξ for a soap film has a simple form:

$$\Delta\xi(t) \equiv \xi - \xi_a = \xi_s(t) + \xi_c, \tag{6}$$

where $\xi_s(t)$ is the sidewall contribution from the soap film with a finite thickness $\ell(t)$. When the value of ℓ becomes small enough at the later stage of draining ($\ell < 35$ nm), the sidewall correction $\xi_s(t)$ is negligibly small compared with ξ_c. In this thin film limit, we have $\Delta\xi_\infty \simeq \xi_c$.

To further study the effect of the film viscosity η on $\Delta\xi_\infty$, we measure $|z(f)|^2$ for soap films with different viscosities. Figure 6 shows how the measured $|z(f)|^2$ changes with η. A thin glass fiber with $d = 1.1\,\mu$m is used, and all the measurements are made at the later stage of the draining. When the soap film reaches the thin film limit with

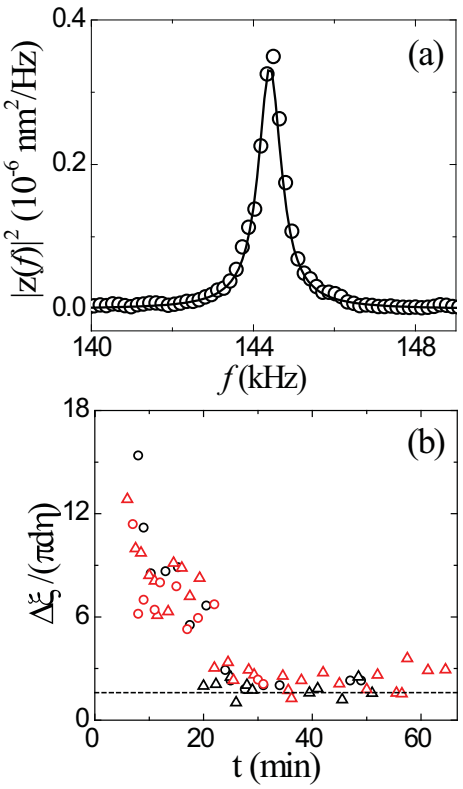

FIG. 5. (Color online) (a) Measured power spectrum $|z(f)|^2$ when a glass fiber intersecting a thin soap film with $\eta = 1.65$ cP (black circles). The solid line shows a fit to Eq. (4) with $\xi = 6.0 \times 10^{-8}$ Ns/m, $k = 11.44$ N/m, and $m = 1.39 \times 10^{-8}$ g. (b) Measured net friction coefficient $\Delta\xi(t)$ as a function of draining time t for a soap film with viscosity $\eta = 1.65$ cP. In the plot, $\Delta\xi$ is normalized by $\pi d\eta$. The measurements are made using an FTS-coated fiber of diameter $d = 1.5\,\mu$m (black symbols) and a cleaned glass fiber of diameter $d = 1.1\,\mu$m (red symbols). For each fiber the measurements are repeated twice (circles and triangles). The dashed line is a plot of $\Delta\xi/(\pi d\eta) = 2\alpha$ with $\alpha = 1.1$.

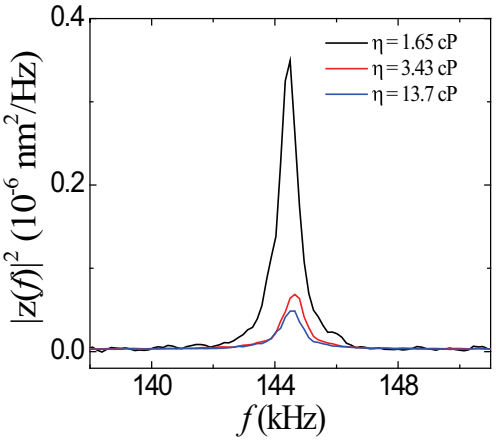

FIG. 6. (Color online) Variations of the measured $|z(f)|^2$ for soap films with different viscosities: $\eta = 1.65$ cP (black curve), 3.43 cP (red curve), and 13.7 cP (blue curve). All the measurements are made when the soap film reaches the thin film limit with $\ell < 35$ nm.

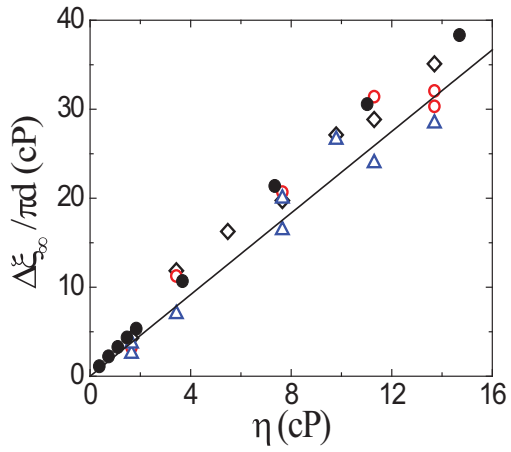

FIG. 7. (Color online) Measured contact line friction per unit length $\Delta\xi_\infty/\pi d$ as a function of viscosity η of the soap film. Three glass fibers with different surface treatments are used: cleaned bare glass fiber with $d = 1.1\ \mu$m (black diamonds), FTS-coated glass fiber with $d = 1.5\ \mu$m (red circles), and DPPC-coated glass fiber with $d = 2.6\ \mu$m (blue triangles). The solid line is a linear fit of Eq. (7) to all the data points with $\alpha = 1.1 \pm 0.3$. The black solid circles are the numerical simulation results obtained at $\theta = 30^\circ$.

$\ell < 35$ nm, the measured $|z(f)|^2$ remains unchanged with time as shown by the plateau region in Fig. 5(b). For soap films with $\eta \geqslant 8$ cP, a filter paper soaked with a small amount of the same soap solution is used to speed up the draining. It is seen that the resonant peak changes continuously with increasing η; the frequency peak broadens while the peak height decreases and peak position shifts to lower frequencies. This behavior is well described by Eq. (4).

By integrating Eq. (4), one finds the mean-square value of contact line fluctuations is given by the equipartition theorem, $k\langle z^2(t)\rangle_t = k_B T$. For $k = 11.4$ N/m, we have $\langle z^2(t)\rangle_t^{1/2} \simeq 1.9 \times 10^{-2}$ nm. The corresponding drag force is $f_d \simeq \xi\omega_0\langle z^2(t)\rangle_t^{1/2} \simeq 1.0$ pN, and the capillary number $\mathrm{Ca} \simeq \eta\omega_0\langle z^2(t)\rangle_t^{1/2}/\gamma \simeq 1.2 \times 10^{-6}$ for the soap film with $\gamma = 23.2$ mN/m, $\xi = 6 \times 10^{-8}$ Ns/m, $\omega_0 = 2\pi \times 144$ kHz, and $\eta = 1.65$ cP. These numbers reveal the tremendous sensitivity of the technique useful for the study of the contact line dynamics.

Figure 7 shows the asymptotic value of the measured contact line friction per unit length $\Delta\xi_\infty/\pi d$ as a function of viscosity η of the soap film. Three glass fibers with different surface treatments are used in the experiment. All the data points for different fibers with varying diameters d and resonant frequencies ω_0 and for soap films with different contact angles θ collapse into a single master curve, which can be well described by a linear function,

$$\Delta\xi_\infty = 2\xi_c = 2\alpha\pi d\eta. \tag{7}$$

The solid line is a linear fit of Eq. (7) to the data points with $\alpha = 1.1 \pm 0.3$. This result is in excellent agreement with Eq. (1), which was obtained for a liquid-air interface [13]. The obtained values of ξ_c also agree well with the numerical simulation results (black solid circles) based on the phase field model under the generalized Navier boundary conditions (see more discussions below). The universal behavior of the measured ξ_c for different fluid systems with various contact angles and surface tensions thus demonstrates unequivocally that ξ_c given in Eq. (7) is indeed associated with a fluctuating contact line in regime (i).

V. FURTHER ANALYSIS AND DISCUSSIONS

Loewenberg [27] has carried out a numerical study of the friction coefficient ξ for an oscillating cylinder of varying length ℓ and diameter d fully immersed in an unbounded fluid (without a contact line). Figure 8 shows the numerically calculated $\xi/(\pi d\eta)$ (blue circles) as a function of cylinder aspect ratio $\Gamma \equiv \ell/d$. The red circle is obtained from the analytical result [28] for an infinitely thin disk of diameter d oscillating normal to its circular plane. The numerical data can be well described by the linear function, $\xi/(\pi d\eta) = 3.27 + 1.74\Gamma$ (solid line). It is seen that the red circle represents a nice asymptotic value of the numerically calculated $\xi/(\pi d\eta)$ at the $\Gamma = 0$ limit without any noticeable jump or discontinuation at the scale of our interest. The dashed line in Fig. 8 is obtained by subtracting out the contribution of the two end surfaces of the cylinder [i.e., the intercept value at $\Gamma = 0$ (red circle)] from the solid line. It can be used to estimate the sidewall contribution $\xi_s \simeq 1.74\Gamma(\pi d\eta)$ in Eq. (6). For a glass fiber of $d = 1.5\ \mu$m intersecting a soap film of thickness ℓ, ξ_s becomes comparable to ξ_c in Eq. (7) (with $\alpha = 1.1$), when $\Gamma \simeq 0.63$ or $\ell \simeq 0.95\ \mu$m. At the thin film limit ($\ell < 35$ nm), we have $\xi_s/(\pi d\eta) \leqslant 0.04$, which is indeed negligibly small compared to the contact line friction $\xi_c/(\pi d\eta) \simeq 1.1$. Thus, ξ_s can indeed be omitted in Eq. (6) at the thin film limit.

While we measure ξ_c through contact line fluctuations, ξ_c is actually an intrinsic property of the MCL and can be realized through a macroscopic flow. Recently, Gao *et al.* [13,29] conducted a direct numerical simulation (DNS) of a two-dimensional two-phase (fluid and gas) flow between two parallel plates under a constant speed U_0 and the third

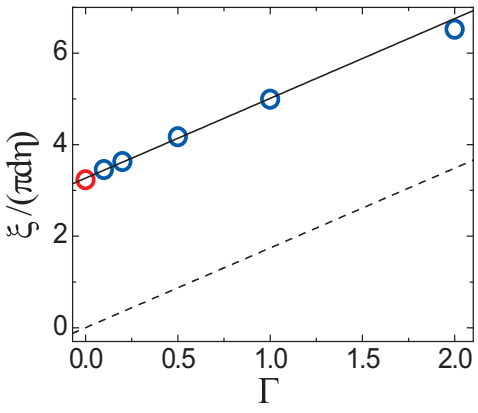

FIG. 8. (Color online) Numerically calculated $\xi/(\pi d\eta)$ as a function of cylinder aspect ratio Γ for $d = 1.5\ \mu$m, $\eta = 1.76$ cP, and $\omega_0 = 2\pi \times 130$ kHz. The blue circles are obtained for a cylinder ($\Gamma \neq 0$) and the red circle is obtained for a indefinitely thin disk. The solid line is a linear fit to the circles: $\xi/(\pi d\eta) = 3.27 + 1.74\Gamma$. The dashed line shows the function $\xi_s/(\pi d\eta) = 1.74\Gamma$, for the sidewall contribution only.

dimension of the flow parallel to the contact line was assumed to be homogeneous. The DNS study was carried out by solving the phase field model of coupled incompressible Navier-Stokes equation and Cahn-Hilliard equation under the generalized Navier boundary conditions [11,16,17] using a gradient stable scheme [30]. In the simulation, the tangential velocity profile $v_x(x)$ at the solid wall was obtained as a function of distance x away from the contact line, where the x axis is along the flow direction. From the obtained $v_x(x)$, one can compute the coefficient $\alpha = \int [v_x(x)/U_0]^2 d(x/\ell_s)$ in Eq. (7), where the slip length ℓ_s (=10 nm) was a fixed input parameter.

The (black) solid circles in Fig. 7 are the calculated $2\xi_c/(\pi d) \equiv 2\alpha\eta$ at $\theta = 30^\circ$. Each value of $2\xi_c/(\pi d)$ was obtained by integrating the normalized dissipation rate $(2\eta/\ell_s)[v_x(x)/U_0]^2$ over the core region $x/\ell_s \leqslant 8$. It was found [31] that the normalized wall velocity $v_x(x)/U_0$ is a scaling function of x/ℓ_s, which slips mainly in the core region $x/\ell_s \lesssim 8$ for all of the fluids used with varying viscosities from 0.37 to 18.4 cP. The dissipation in the partial slip region and beyond is too small to be detected by the hanging fiber. Figure 7 clearly reveals that the numerical results are in good agreement with the measured $2\xi_c/(\pi d)$.

To avoid the dissipation divergence of the MCL, de Gennes *et al.* [32] introduced the cutoff length a, as shown in the inset of Fig. 1(a), and calculated the hydrodynamic friction coefficient $\xi_{\rm hd}$ in regime (ii) away from the contact line,

$$\xi_{\rm hd} \simeq (3\ln(L/a)/\theta)\pi d\eta \equiv \alpha_{\rm hd}\pi d\eta, \tag{8}$$

for liquids with a small contact angle θ. The calculated $\alpha_{\rm hd}$ in Eq. (8) is $\alpha_{\rm hd} \simeq 27.6/\theta$ for $L \simeq 10\,\mu$m. This value of $\alpha_{\rm hd}$ is about 100 times larger than the measured α for liquids with $\theta \simeq 20^\circ$ and even becomes divergent for liquids with $\theta = 0^\circ$. Clearly, the calculated $\xi_{\rm hd}$ for regime (ii) does not apply to the measured ξ_c as shown in Fig. 7, further confirming that the measured ξ_c does not result from the hydrodynamic friction in regime (ii), made possible by the asymptotic nanometer thickness of the soap film.

A different approach to modeling the contact line dissipation is the molecular kinetic theory (MKT) of Blake and Haynes [4,33]. In MKT, the motion of the contact line in regime (i) is described as a molecular hopping event over an energy barrier E_0 under the influence of an applied force acting on the contact line due to the unbalanced capillary force,

$$f_{\rm un} = \gamma(\cos\theta_0 - \cos\theta_d)\lambda, \tag{9}$$

where θ_d is the dynamic contact angle, which differs from its equilibrium value θ_0, and λ is a length scale characterizing the distance between adsorption sites on the solid surface. This unbalanced capillary force increases the forward hopping rate k^+, reducing the backward hopping k^-, and gives rise to a net velocity of the contact line, $V = (k^+ - k^-)\lambda$.

For a small force $f_{\rm un}$, V was found to be proportional to $f_{\rm un}$ and the inverse of the proportionality constant is the friction coefficient of the contact line, which has the form [33–35]

$$\xi_{\rm mkt} \simeq \left[\left(\frac{b^3}{\lambda^3}\right)e^{E_0/k_BT}\right]\pi d\eta \equiv \alpha_{\rm mkt}\pi d\eta, \tag{10}$$

where b^3 is the volume of a liquid molecule. For a smooth solid surface, λ is of the order of the lattice constant of the solid crystal and thus one has $b^3/\lambda^3 \simeq 1$. The energy barrier height E_0 is typically of the order of the adhesion energy $E_0 \simeq \lambda^2(\gamma_{\rm sv} + \gamma - \gamma_{\rm sl}) = \gamma\lambda^2(1 + \cos\theta_0)$ [35], where $\gamma_{\rm sv}$ and $\gamma_{\rm sl}$ are, respectively, the tensions of the solid-vapor and solid-liquid interfaces, and we have assumed that the adsorption sites are closely packed over the solid surface. For $\lambda = 0.54$ nm (lattice constant of quartz), $\theta_0 = 0^\circ$, and $\gamma = 72.8$ mN/m (surface tension of water-air interface), we have $E_0/k_BT \simeq 10.5$ and $\alpha_{\rm mkt} = e^{E_0/k_BT} \simeq 3.6 \times 10^4$. If one assumes $E_0 \simeq \lambda^2(\gamma_{\rm sv} - \gamma_{\rm sl}) = \lambda^2\gamma\cos\theta_0$ [35], we find $E_0/k_BT \simeq 5.25$ and $\alpha_{\rm mkt} = e^{E_0/k_BT} \simeq 190$. This value of $\alpha_{\rm mkt}$ is still ~170 times larger than the measured α in Fig. 7. Note that $E_0/k_BT \simeq 5.25$ is approximately the lower bound of the energy range, in which the Arrhenius-Kramers rate equation is obtained under the steepest descent approximation [36]. For smaller values of E_0, the expression of the rate equation is not accurate [37].

Equation (10) has been used recently to analyze a number of data sets obtained from the drop spreading experiments, in which a high-speed camera was used to record the apparent contact angle $\theta_{\rm ap}(t)$ and radius $R(t)$ of the deposited drop on a flat substrate, as it evolves with time t. For a single set of data obtained from spontaneous spreading of aqueous glycerol drops on a flat glass substrate, the fitted value of $\alpha_{\rm mkt}$ was found to be $\alpha_{\rm mkt} = 273$ [34]. From a collection of 20 data sets resulting from different drop spreading systems, the fitted value of $\alpha_{\rm mkt}$ was found to be $\alpha_{\rm mkt} = 7.82 \times 10^4$ [35]. The obtained values of $\alpha_{\rm mkt}$ are much larger than the measured α in Fig. 7. There are several causes that may contribute to the large value of the fitted $\alpha_{\rm mkt}$. First, the friction coefficient obtained from the drop spreading experiments includes both the contributions from the bulk fluid [i.e., from regime (ii)] and from the contact line [i.e., from regime (i)]; both are viscous contributions and thus are proportional to fluid viscosity η. Because the contact area on the substrate occupied by the bulk fluid of the drop is much larger than that occupied by the contact line, the obtained friction coefficient from the drop spreading experiments is overwhelmingly dominated by the bulk contribution from regime (ii). The calculated $\xi_{\rm mkt}$ (or $\alpha_{\rm mkt}$) in Eq. (10), on the other hand, is for the contact line friction from regime (i).

Second, the friction coefficient from the drop spreading experiments was obtained using the apparent (macroscopic) contact angle $\theta_{\rm ap}$, whereas θ_d in Eq. (9) is a truly microscopic contact angle defined at the contact line. Because of surface roughness and chemical heterogeneities, θ_d is fundamentally different from $\theta_{\rm ap}$ [3,4]. In fact, the present experiment is the first one to directly measure the contact line friction in regime (i) by deliberately using a nanometer thin soap film, so that the contribution of the bulk fluid to the viscous damping of the soap film is negligibly small. Because the friction measurement is conducted at equilibrium using the fluctuation-dissipation theorem [15] without involving a macroscopic flow, the measured contact line friction shown in Fig. 7 is insensitive to the contact line pinning and other surface complications.

Furthermore, Gao *et al.* calculated the energy dissipation ϵ_o (per oscillation period) of a hypothetical capillary wave due to the small amplitude oscillation of the vertical fiber [29]. By solving the incompressible Navier-Stokes equation at the liquid-air interface, an analytical solution of the equation

was obtained at the inviscid limit [38]. From the obtained velocity profile, an upper bound of the energy dissipation $\epsilon_o \lesssim \gamma \langle z^2 \rangle_t$ was obtained, assuming that the energy associated with the capillary wave is all dissipated. Here γ is the tension of the liquid-air interface. The obtained value of ϵ_o for $\langle z^2 \rangle_t^{1/2} \simeq 2 \times 10^{-2}$ nm and $d = 2.3\,\mu$m is $\epsilon_o \simeq 1.1 \times 10^{-22}$ J, which is 76 times smaller than the thermal energy $(1/2)k_BT$ of the vibrating fiber. This calculation thus confirmed that the damping caused by a hypothetical capillary wave to the oscillating fiber is negligibly small when compared with the measured ξ_c shown in Fig. 7.

VI. CONCLUSION

We have carried out a systematic study of (moving) contact line dissipation by directly measuring the friction coefficient ξ_c of two fluctuating contact lines formed on a fiber surface when a long glass fiber intersects the two water-air interfaces of a thin soap film. The glass fiber of diameter d in the range of 0.4–4 μm and length 100–300 μm is glued onto the front end of a rectangular cantilever used for atomic force microscopy (AFM). As a sensitive mechanical resonator, the vertical motion of the hanging fiber probe is well described by the Langevin equation given in Eq. (3). Minute changes of the viscous damping caused by the thin soap film (i.e., by thermal fluctuations of the two contact lines about their equilibrium positions on the fiber surface) are detected in the measured resonant power spectrum $|z(\omega)|^2$, as the fluctuation and dissipation are intrinsically linked together by the fluctuation-dissipation theorem.

By measuring the broadening of the resonant peak of the hanging fiber probe with varying viscosity η of the soap film and different surface treatments of the glass fiber, we confirm that the contact line dissipation obeys a universal scaling law as shown in Eq. (7), where the coefficient $\alpha = 1.1 \pm 0.3$. This result is obtained at the thin film limit, in which the contribution of the bulk fluid to the viscous damping of the soap film is negligibly small. Furthermore, the universal scaling law is tested with two different liquid-solid contact angles of $\theta \simeq 0^\circ$ and $\theta \simeq 20^\circ$, and the results are found to be insensitive to the change of θ. The experimental result is in good agreement with the numerical result based on the phase field model under the generalized Navier boundary conditions [13].

The establishment of the scaling law given in Eq. (7) for the contact line dissipation has several important implications. First, as a universal scaling law applicable to different fluid systems with different viscosities and contact angles, it provides a rigorous relationship which can be used to test various microscopic models for moving contact line (MCL). Second, it sets up an intrinsic bound for the dissipation of the MCL in regime (i), which is useful for evaluating relevant molecular parameters associated with the MCL, such as the slip length for different fluids. Finally, the understanding of contact line dissipation provides a solid foundation for the further study of other liquid interfaces of practical interest, such as those coated with polymers, surfactant, and lipids.

ACKNOWLEDGMENTS

We have benefited from illuminating discussions with T.-Z. Qian, X.-P. Wang, J.-J. Benattar, and D. Beck. This work was supported by the Research Grants Council of Hong Kong SAR under Grants No. HKUST 605013 (P.T.), No. 604211 (P.S.), and No. SRFI11/SC02 (P.S.).

[1] L. Leger and J. F. Joanny, Rep. Prog. Phys. **55**, 431 (1992).
[2] D. Quéré, Annu. Rev. Mater. Res. **38**, 71 (2008).
[3] D. Bonn, J. Eggers, J. Indekeu, J. Meunier, and E. Rolley, Rev. Mod. Phys. **81**, 739 (2009).
[4] J. Snoeijer and B. Andreotti, Annu. Rev. Fluid Mech. **45**, 269 (2013).
[5] E. B. V. Dussan and S. H. J. Davis, J. Fluid Mech. **65**, 71 (1974).
[6] T. Ondarcuhu and M. Veyssie, Nature **352**, 418 (1991).
[7] J. A. Marsh, S. Garoff, and E. B. Dussan V., Phys. Rev. Lett. **70**, 2778 (1993).
[8] Q. Chen, E. Ramé, and S. Garoff, J. Fluid Mech. **337**, 49 (1997).
[9] J. Koplik, J. R. Banavar, and J. F. Willemsen, Phys. Rev. Lett. **60**, 1282 (1988).
[10] P. A. Thompson and M. O. Robbins, Phys. Rev. Lett. **63**, 766 (1989).
[11] T. Qian, X.-P. Wang, and P. Sheng, Phys. Rev. Lett. **93**, 094501 (2004).
[12] J. D. Coninck and T. Blake, Annu. Rev. Mater. Res. **38**, 1 (2008).
[13] S. Guo, M. Gao, X. Xiong, Y. J. Wang, X. Wang, P. Sheng, and P. Tong, Phys. Rev. Lett. **111**, 026101 (2013).
[14] X. Xiong, S. Guo, Z. Xu, P. Sheng, and P. Tong, Phys. Rev. E **80**, 061604 (2009).
[15] R. Kubo, Rep. Prog. Phys. **29**, 255 (1966).
[16] T. Qian, X.-P. Wang, and P. Sheng, Phys. Rev. E **68**, 016306 (2003).
[17] T. Qian, X.-P. Wang, and P. Sheng, J. Fluid Mech. **564**, 333 (2006).
[18] H.-L. Ma, J. Jimenez, and R. Rajagopalan, Langmuir **16**, 2254 (2000).
[19] F. Reif, *Fundamentals of Statistical and Thermal Physics* (McGraw-Hill, Auckland, 1985).
[20] S. Guo, X. Xiong, Z. Xu, P. Sheng, and P. Tong, Chinese Phys. B **23**, 116802 (2014).
[21] P. D. T. Huibers and D. O. Shah, Langmuir **13**, 5995 (1997).
[22] C. W. McConlogue and T. K. Vanderlick, Langmuir **13**, 7158 (1997).
[23] P. Silberzan, L. Leger, D. Ausserre, and J. J. Benattar, Langmuir **7**, 1647 (1991).
[24] J. B. Brzoska, I. B. Azouz, and F. Rondelez, Langmuir **10**, 4367 (1994).
[25] I. B. Ivanov, *Thin Liquid Film* (Marcel Dekker Inc., New York, USA, 1988).
[26] P. Poulin, F. Nallet, B. Cabane, and J. Bibette, Phys. Rev. Lett. **77**, 3248 (1996).
[27] M. Loewenberg, Phys. Fluids A **5**, 3004 (1993).
[28] W. Zhang and H. A. Stone, J. Fluid Mech. **367**, 329 (1998).

[29] M. Gao, Ph.D. thesis, Hong Kong University of Science and Technology, 2012.
[30] M. Gao and X.-P. Wang, J. Comput. Phys. **231**, 1372 (2012).
[31] See Supplemental Material of Ref. [13], Sec. II, Direct Numerical Simulation at http://link.aps.org/supplemental/10.1103/PhysRevLett.111.026101 for more details.
[32] P. de Gennes, F. Brochard-Wyart, and D. Quere, *Capillarity and Wetting Phenomena: Drops, Bubbles, Pearls, Waves* (Springer, Berlin, 2004).
[33] T. D. Blake and J. Haynes, J. Colloid Interface Sci. **30**, 421 (1969).
[34] D. Duvivier, D. Seveno, R. Rioboo, T. D. Blake, and J. D. Coninck, Langmuir **27**, 13015 (2011).
[35] D. Duvivier, T. D. Blake, and J. D. Coninck, Langmuir **29**, 10132 (2013).
[36] P. Hanggi, P. Talkner, and M. Borkovec, Rev. Mod. Phys. **62**, 251 (1990).
[37] X.-G. Ma, P.-Y. Lai, and P. Tong, Soft Matter **9**, 8826 (2013).
[38] P. Sheng and M. Zhou, Phys. Rev. A **45**, 5694 (1992).